Journal of Solid State Chemistry **157,** 261–273 (2001)
doi:10.1006/jssc.2000.9049, available online at http://www.idealibrary.com on IDEAL®

Effect of Cationic Substitutions on Ferroelectric Properties of $Pb_5Ta_{10}O_{30}$: Generation of the Relaxor Behavior

V. Hornebecq,[1] C. Elissalde, P. Gravereau, E. Lebraud, and J. Ravez

Institut de Chimie de la Matière Condensée de Bordeaux, ICMCB - CNRS [UPR 9048], 87, Av. Dr A. Schweitzer, 33608 Pessac Cedex, France

Received July 17, 2000; in revised form November 14, 2000; accepted November 15, 2000; published online February 19, 2001

New compositions derived from $Pb_5Ta_{10}O_{30}$ have been synthetized to study the influence of cationic substitutions [heterovalent ($Pb^{2+} \rightarrow La^{3+}$ and $Pb^{2+} \rightarrow K^{+}$) and homovalent ($Pb^{2+} \rightarrow Ba^{2+}$ and $Pb^{2+} \rightarrow Ca^{2+}$)] on its ferroelectric properties. The ferroelectric behavior of each composition was evidenced by way of dielectric measurements as a function of both temperature and frequency. Structure determinations and refinements were also performed to determine which crystallographic sites are occupied by the substituted cations, Whatever the nature of the substitution, the relaxor behavior is induced by a weak rate of substitution. Furthermore, except in the case of the calcium-containing composition, no significative difference was found concerning crystallographic data. All the results obtained are compared with those described in the literature and discussed in terms of charge, ionic radius, and steric effect. © 2001 Academic Press

Key Words: **ceramics; ferroelectric; cationic substitution; relaxor behavior; structure determination.**

1. INTRODUCTION

Among ferroelectric compounds, two types of behavior can be distinguished: the classical behavior associated with both a sharp phase transition and a temperature maximum of the real part of the permittivity ε'_r (temperature of Curie T_C), which is not dependent on frequency, and the relaxor behavior associated with a diffuse phase transition and a temperature maximum of $\varepsilon'_r(T_m)$, which increases with increasing frequency.

From a structural point of view, the first condition known to induce relaxor behavior is the presence of two different cations in the same crystallographic site (1). In lead-containing perovskites or tetragonal tungsten bronzes (TTB), an additional condition was evidenced: the displacement of lead atoms from their normal position in the considered site (2, 3). Recently, the origin of the relaxor behavior was investigated in compositions with a tetragonal tungsten bronze structure by way of a comparative crystallographic study between a classical composition ($Pb_{2.5}K_3Li_2\ Ta_{10}O_{30}$) and a relaxor one ($Pb_{3.75}K_{1.5}LiTa_{10}O_{30}$) (4). The only qualitative difference between the two compositions was the proportion of lead atoms in the pentagonal A2 sites. This observation led to another additional condition necessary for the existence of the relaxor behavior in such compounds: the ratio Pb/(Pb + K) in the A2 sites must be greater than 0.5 (4).

The aim of this study is to investigate the influence of various substitutions on the dielectric properties of lead metatantalate ($Pb_5Ta_{10}O_{30}$). This compound is a classical ferroelectric with a Curie temperature close to 540 K (5, 6). It crystallizes in the TTB structure with cell parameters equal to $a = b = 12.5007(3)$ Å and $c = 3.8766(2)$ Å. Two different types of substitutions are considered: heterovalent substitutions [($Pb^{2+} \rightarrow La^{3+}$) and ($Pb^{2+} \rightarrow K^{+}$)] and homovalent substitutions [($Pb^{2+} \rightarrow Ba^{2+}$) and ($Pb^{2+} \rightarrow Ca^{2+}$)]. The preparation of samples, ferroelectric properties, and structure determinations are reported in the present work. Furthermore, results obtained are compared with those evidenced in other lead-containing compounds with either a perovskite- or a TTB-type structure.

2. EXPERIMENTAL DETAILS

2.1. Sample Preparation

Lanthanum-containing ceramics with composition $Pb_{5(1-x)}La_{10x/3}Ta_{10}O_{30}$ ($x = 0.075$, 0.10, and 0.15) were prepared using the conventional solid state process. The required quantities of La_2O_3 (Reacton 99.99%), PbO (Merck 99.5%), and Ta_2O_5 (Cérac 99.95%) were weighted out and mixed in a dry box for 45 min. The resultant powder was pressed into discs of 13-mm diameter and then calcined in an air atmosphere for 12 h. The corresponding pellets were ground mechanically for 4 h and then sintered for 5 h. Potassium-containing ceramics with composition $Pb_{5(1-x)}K_{10x}Ta_{10}O_{30}$ ($x = 0.10$ and 0.15) were prepared

[1] To whom correspondence should be addressed. E-mail: hornebec@icmcb.u-bordeaux.fr. Fax: + 33-5-56842761.

0022-4596/01 $35.00

TABLE 1
Temperatures of Calcination ($T_{calc.}$) and Sintering ($T_{sint.}$) for All Compositions Studied

Composition	$T_{calc.}$	$T_{sint.}$
$Pb_{4.625}La_{0.25}Ta_{10}O_{30}$	1100	1430
$Pb_{4.5}La_{0.33}Ta_{10}O_{30}$	1125	1430
$Pb_{4.25}La_{0.50}Ta_{10}O_{30}$	1150	1430
$Pb_{4.5}KTa_{10}O_{30}$	1000	1430
$Pb_{4.25}K_{1.5}Ta_{10}O_{30}$	1000	1430
$Pb_{4.5}Ba_{0.5}Ta_{10}O_{30}$	1100	1405
$Pb_4BaTa_{10}O_{30}$	1125	1405
$Pb_{4.5}Ca_{0.5}Ta_{10}O_{30}$	1150	1420

using the same process described above. For barium-containing ceramics with $Pb_{5(1-x)}Ba_{5x}Ta_{10}O_{30}$ ($x = 0.10$ and 0.20) compositions and $Pb_{4.5}Ca_{0.5}Ta_{10}O_{30}$ composition, the initial reaction mixture was ground, calcined, and sintered under an oxygen atmosphere for 12 and 5 h, respectively. Table 1 reports the calcination and sintering temperatures for all these compositions. For all samples, weight losses after sintering were less than 1%. The diameter shrinkage and the compactness lie between 18 and 20% and between 92 and 93%, respectively. X-ray diffraction analysis of each ceramic confirms the presence of a single phase with a TTB-type structure.

2.2. Dielectric Measurements

Ferroelectric measurements were performed on ceramic discs. Electrodes were formed by depositing gold on the top and bottom of circular surfaces by sputtering. In the frequency range 20–2×10^5 Hz, the permittivities values were derived from the capacitance and dielectric losses. Measurements were made under vacuum in the temperature range 100, 600 K using a Wayne-Kerr 6425 component analyzer.

2.3. Structure Determination

X-ray diffraction data for the Rietveld analysis were collected using a Philips PW 3040/00 X′PERT MPD device in Bragg-Brentano geometry, using diffracted beam graphite monochromator Cu$K\alpha$ radiation (7). Data were collected over the angular range $10^\circ \leq 2\theta \leq 120^\circ$ with a 0.02° step and a fixed counting time of 30 s. Refinements were performed on the basis of the results obtained previously for $Pb_{3.75}K_{1.5}LiTa_{10}O_{30}$ using the program FULLPROF (9). The background level was fitted with a five-order polynomial function and the peak shape with a pseudo-Voigt function. The angular dependence of the peak full-width at half-maximum was defined by the function determined by Caglioti *et al.* (10).

3. RESULTS AND DISCUSSION

3.1. Heterovalent Substitutions: $Pb^{2+} \rightarrow La^{3+}$ and $Pb^{2+} \rightarrow K^+$

The two cations were chosen because of their difference in charge and also because of their difference in ionic radius (C.N. 12) ($r[La^{3+}] = 1.36$ Å, $r[K^+] = 1.64$ Å, and $r[Pb^{2+}] = 1.49$ Å) (8).

3.1.1. Ferroelectrics Properties

The Curie temperature, T_C (or the temperature of the maximum of ε'_r, T_m), was determined for each composition at 10^3 Hz. For lanthanum- or potassium-containing

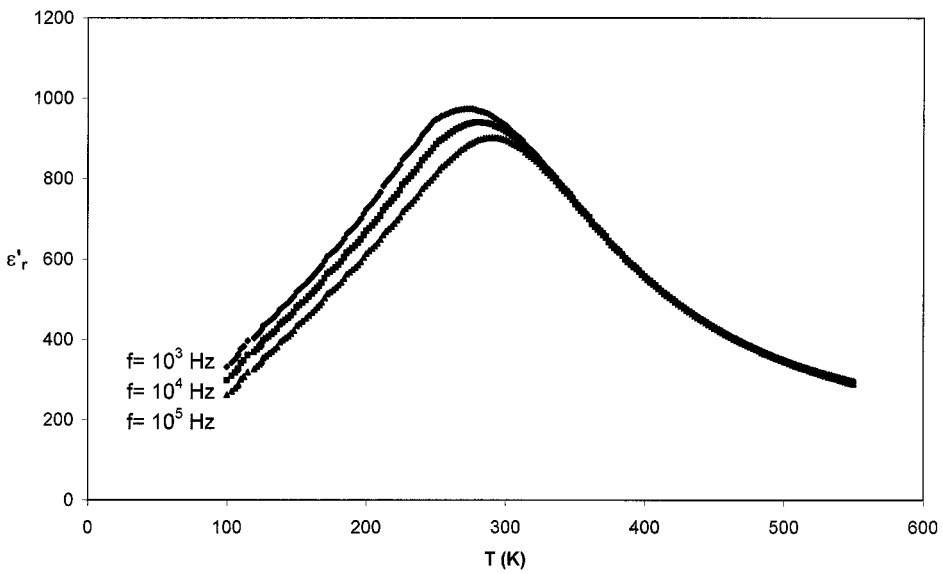

FIG. 1. Temperature dependence of ε'_r at various frequencies for $Pb_{4.25}La_{0.5}Ta_{10}O_{30}$ ($x = 0.15$) composition.

TABLE 2
Values of T_C or T_m, Ferroelectric Behavior, and Values of ΔT_m for Lanthanum- and Potassium-Containing Ceramics

	$Pb_{5(1-x)}La_{10x/3}Ta_{10}O_{30}$			$Pb_{5(1-x)}K_{10x}Ta_{10}O_{30}$	
Composition	$x = 0.075$	$x = 0.10$	$x = 0.15$	$x = 0.10$	$x = 0.15$
T_C or T_m (K)	380	360	275	290	220
Ferroelectric behavior	Classical	Relaxor	Relaxor	Relaxor	Relaxor
ΔT_m(K)	0	5	17	15	20

compositions, T_C (or T_m) decreases as x increases (Table 2). The temperature dependence of the real part of the permittivity, ε'_r, at various fixed frequencies allowed the ferroelectric behavior (classical or relaxor) to be determined for each composition (Fig. 1 for $Pb_{4.25}La_{0.5}Ta_{10}O_{30}$). The type of ferroelectric behavior as well as the value of ΔT_m [T_m (10^5 Hz)–T_m(10^3 Hz)] (reflecting the amplitude of the relaxor behavior) for relaxor compositions are given in Table 2.

To confirm the existence of the relaxor behavior, each sample was analyzed over the frequency range (20–2×10^5 Hz) in the ferroelectric phase, $T = T_m - 60$ K, and in the paraelectric phase, $T = T_m + 80$ K. For all relaxor compositions, as the frequency increases, the variation of ε'_r versus log f exhibits a continous decrease whereas a diffuse maximum of ε''_r appears for $T < T_m$. For $T > T_m$, this phenomenon disappears; there is no variation of both ε'_r and ε''_r with frequency and the values of ε''_r are very weak. These results are in agreement with the relaxor behavior, which exists only in the ferroelectric phase ($T < T_m$). Figures 2 and 3 represent the variation of ε'_r as a function of frequency at the two considered temperatures.

3.1.2. Structure Determination and Refinements

In reference to a previous study of $Pb_{3.75}K_{1.5}LiTa_{10}O_{30}$, the determination of the site(s) occupied by lanthanum or potassium atoms in the structure is a necessary step for the understanding of the influence of heterovalent substitution on the relaxor behavior (4). Among lanthanum- and potassium-containing relaxor compositions, the $Pb_{4.25}La_{0.5}Ta_{10}O_{30}$ and $Pb_{4.5}KTa_{10}O_{30}$ ones were chosen as they present comparable values of ΔT_m.

For both compositions, X-ray diffraction patterns were indexed on the basis of a tetragonal unit cell. The reflection condition [$(0kl)$ $k = 2n$] was compatible with space groups $P4/mbm$, $P\bar{4}b2$, and $P4bm$. In agreement with our previous results on $Pb_{3.75}K_{1.5}LiTa_{10}O_{30}$, refinements are done in the centrosymmetric space group (paraelectric phase) $P4/mbm$ (4). The powder data and experimental conditions are given in Table 3.

The formula by unit prototype cell of the TTB-type structure corresponds to $A1_2A2_4C_4B_{10}O_{30}$ in which A1, A2, C, and B are the 12-, 15-, 9- and 6-fold oxygen anions coordinated sites in the crystal structure. The BO_6 octahedra are linked by theirs corners in such a manner as to form different types of tunnels running through the structure parallel to c (Fig. 4).

$Pb_{4.25}La_{0.5}Ta_{10}O_{30}$. During the preliminary stage of refinements, no assumptions were made regarding the sites $A1$ or $A2$ and the occupancy parameters of lead and lanthanum atoms. Refinements failed if lanthanum atoms

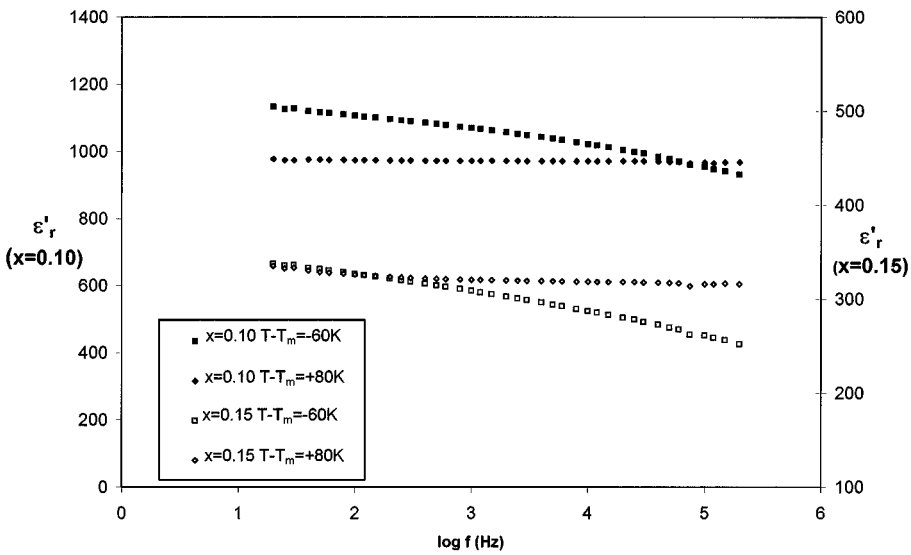

FIG. 2. Frequency variation of ε'_r for lanthanum-containing compositions $x = 0.10$ and $x = 0.15$ at $T < T_m$ and $T > T_m$.

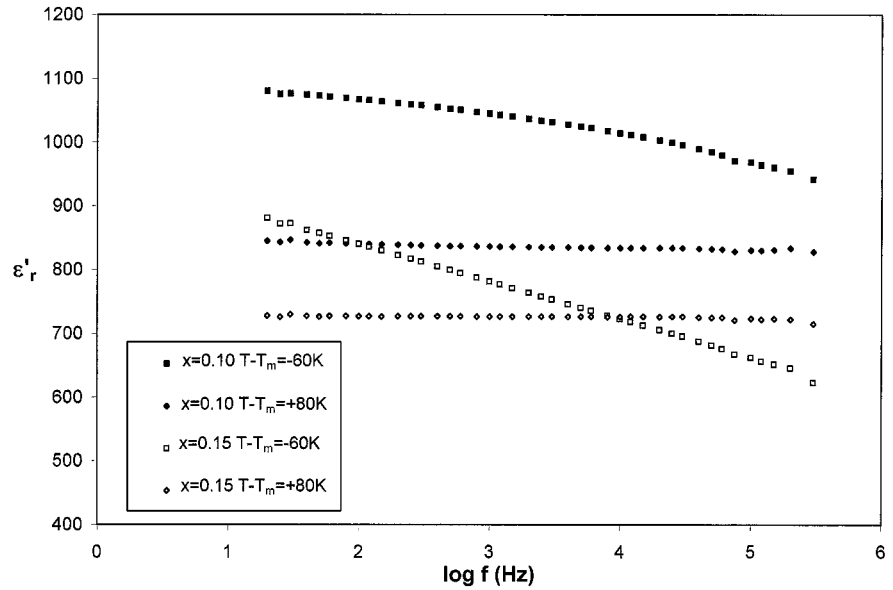

FIG. 3. Frequency variation of ε'_r for potassium-containing compositions $x = 0.10$ and $x = 0.15$ at $T < T_m$ and $T > T_m$.

occupy the $A1$ site [site $2a$ (0, 0, 0)]: such an assumption led to a poor reliability factor and to a negative value of the considered population parameter. The best refinements were obtained with each square $A1$ site occupied only by lead in a normal position [site $2a$ (0, 0, 0)] and each pentagonal site $A2$ partially occupied by either a lanthanum atom in a normal position [site $4g$ (x, $x + \frac{1}{2}$, 0)] or a lead atom in one of the two shifted positions [site $8i$ (x, $x + \frac{1}{2} + \delta$, 0)]. This result is in agreement with the structure determination of $Pb_4K_2Ta_{10}O_{30}$ performed by Sciau *et al.* (11). In fact, the best refinements were obtained for this composition by keeping the K^+ cation on the original special position and by distributing the Pb^{2+} cation on the two positions on

TABLE 3
Powder Crystallographic Data, Experimental Conditions, and Rietveld Data for $Pb_{4.25}La_{0.5}Ta_{10}O_{30}$ and $Pb_{4.5}KTa_{10}O_{30}$

	$Pb_{4.25}La_{0.5}Ta_{10}O_{30}$	$Pb_{4.5}KTa_{10}O_{30}$
Crystallographic data		
Symmetry	Tetragonal	
Existence conditions	$(0kl)$ $k = 2n$	
Space group	$P4/mbm$ (No. 127)	
Unit-cell parameters (Å)	$a = b = 12.4710(1)$	$a = b = 12.5391(1)$
	$c = 3.8724(1)$	$c = 3.9010(1)$
Volume (Å^3)	$V = 602(1)$	$V = 613(1)$
Experimental conditions for data collection		
Radiation	Cu$K\alpha$ ($l = 1.5418$ Å)	
Measuring range	$10^\circ < 2\theta < 120^\circ$	
Step	0.02°	
Integration time	30 s	
Rietveld data		
Program for Rietveld analysis	Fullprof	
Number of independent reflections	285	288
Number of independent parameters	29	29
Function for background level	Polynomial (5 order)	Polynomial (5 order)
Function for peak shape	Pseudo-Voigt	Pseudo-Voigt
($H^2 = U \tan^2\theta + V \tan\theta + W$)	$U = 0.026(2)$	$U = 0.022(2)$
	$V = -0.005(2)$	$V = -0.005(2)$
	$W = 0.005(1)$	$W = 0.005(1)$

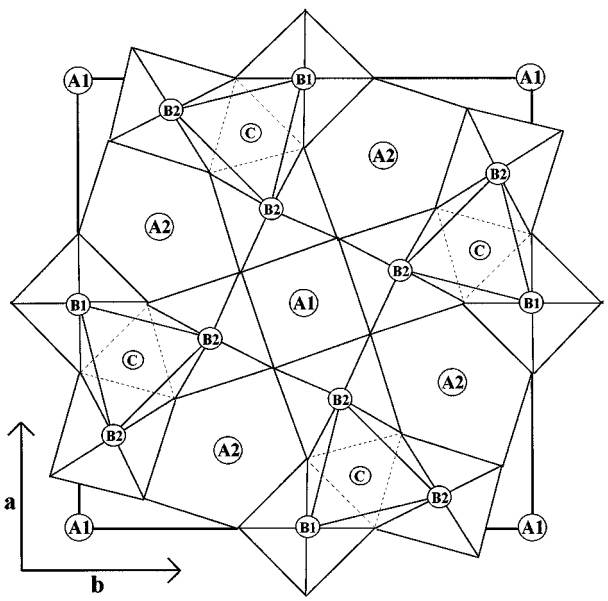

FIG. 4. (001) projection of tetragonal tungsten bronze crystallographic unit cell.

TABLE 4
Atomic Coordinates, Isotropic Thermal Parameters B (Å^2) and Occupancies p in $Pb_{4.25}La_{0.5}Ta_{10}O_{30}$ (Bold) and $Pb_{4.5}KTa_{10}O_{30}$ at 298 K

Atoms	Theoretical valence	Wyckoff site	x	y	z	B	p
Ta(1)	+ 5	2*c*	**0**	**0.5**	**0.5**	**0.05(1)**	**1**
			0	0.5	0.5	0.29(3)	1
Ta(2)	+ 5	8*j*	**0.0739(1)**	**0.2096(1)**	**0.5**	**0.05(1)**	**1**
			0.0748(1)	0.2110(1)	0.5	0.15(3)	1
Pb(1)	+ 2	2*a*	**0**	**0**	**0**	**0.95(14)**	**0.392(1)**
			0	0	0	0.85(8)	0.704(1)
Pb(2)	+ 2	8*i*	**0.1883(2)**	**0.6513(2)**	**0**	**2.04(10)**	**0.432(1)**
			0.1897(3)	0.6472(3)	0	3.49(13)	0.380(1)
La(1)	**+ 3**	**4*g***	**0.2102(16)**	**0.7102(16)**	**0**	**2.04(10)**	**0.124(3)**
K(1)	+ 1	4*g*	0.2139(31)	0.7139(31)	0	3.49(13)	0.244(3)
O(1)	− 2	8*j*	**0.3470(17)**	**0.0035(11)**	**0.5**	**3.1(2)***	**1**
			0.3448(15)	0.0026(12)	0.5	2.3(2)*	1
O(2)	− 2	8*j*	**0.1394(14)**	**0.0578(18)**	**0.5**	**3.1(2)***	**1**
			0.1415(13)	0.0588(16)	0.5	2.3(2)*	1
O(3)	− 2	4*h*	**0.2825(12)**	**0.7825(12)**	**0.5**	**3.1(2)***	**1**
			0.2825(13)	0.7825(13)	0.5	2.3(2)*	1
O(4)	− 2	2*d*	**0**	**0.5**	**0**	**3.1(2)***	**1**
			0	0.5	0	2.3(2)*	1
O(5)	− 2	8*i*	**0.0782(15)**	**0.2078(14)**	**0**	**3.1(2)***	**1**
			0.0786(15)	0.2094(13)	0	2.3(2)*	1

Note. * denotes the average refined value for oxygen atoms.

both sides of the 2-fold axis. The corresponding reliability factors were $R_{Bragg} = 7.8\%$, $cR_p = 16.6\%$, $R_F = 6.9\%$, and $\chi^2 = 1.95$. The final positional coordinates and the final atomic displacements corresponding to the best model are listed in Table 4. Figure 5 gives the observed and calculated X-ray diffraction patterns as well as their differences in $Pb_{4.25}La_{0.5}Ta_{10}O_{30}$ composition.

The interatomic distances for the $Pb_{4.25}La_{0.5}Ta_{10}O_{30}$ composition are reported in Table 5. The Pb–O distances involved in *A*1 sites are of the same order whereas the Pb–O and La–O distances involved in the *A*2 sites are largely distributed from 2.71 to 3.76 Å and from 2.32 to 3.74 Å, respectively. The Ta(1)–O_6 octahedra are slightly distorted whereas Ta(2)–O_6 octahedra are distorted: the apical Ta(2)–O distances are equal whereas the equatorial Ta(2)–O distances are distributed from 1.86 to 2.06 Å and the angles values are different from 90° and 180°.

$Pb_{4.5}KTa_{10}O_{30}$. The results of the structure refinements are very similar to those obtained for the lanthanum-containing composition. The *A*1 sites are occupied only by lead associated to a population parameter (p) equal to 0.70 whereas the *A*2 sites are occupied either by potassium atoms in a normal position 4*g* ($p = 0.24$) or by lead atoms in a shifted position 8*i* ($p = 0.38$). Table 4 reports final positional coordinates and final atomic displacements corresponding to the best model ($R_{Bragg} = 7.5\%$, $cR_p = 16.9\%$, $R_F = 7.05\%$, and $\chi^2 = 2.00$) and interatomic distances are listed in Table 5.

3.1.3. Discussion

Lanthanum-containing compositions. The influence of La doping on dielectric properties was mostly evidenced in lead-containing compositions with a perovskite structure.

The modification of the dielectric properties of lead magnobiate [$Pb(Mg_{1/3}Nb_{2/3})O_3$)] (PMN) ceramics by La doping were studied by de Mathan *et al.* ten years ago (12, 13). PMN is a relaxor ferroelectric and it was shown that La-doped PMN (PLMN) ceramics present a more diffuse phase transition than pure PMN. TEM observations performed on PLMN revealed an increase in the size of the ordered domains. The lanthanum (donor) substitution on the *A* site in the perovskite structure balances the electrical charge of the ordered domains (acceptor) promoting their growth. More recently, structural analysis of PLMN showed that

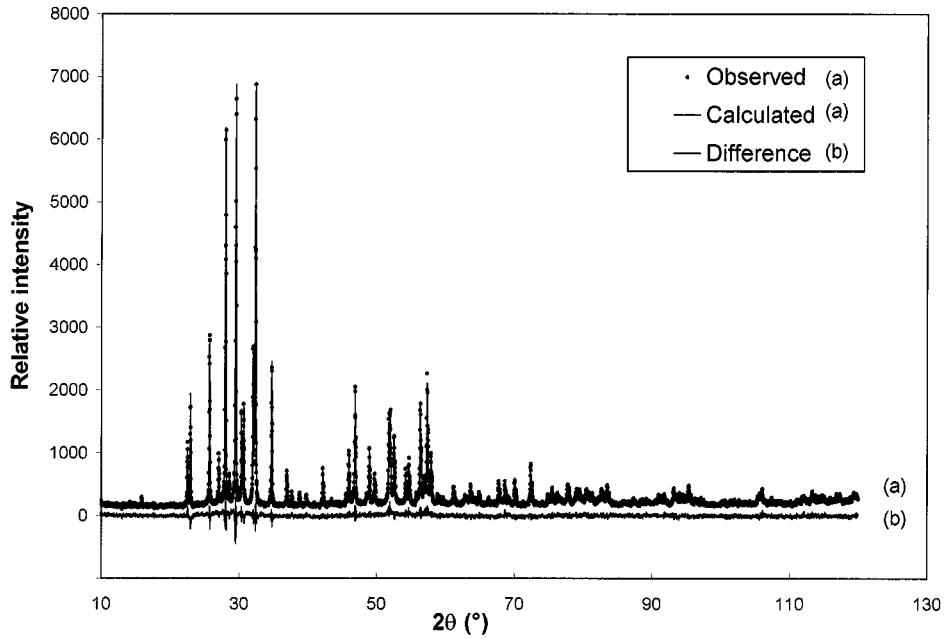

FIG. 5. X-ray diffraction patterns for $Pb_{4.25}La_{0.5}Ta_{10}O_{30}$ ($x = 0.15$) composition.

the ordering changes from complete Nb:Mg ordering to a Nb:($Mg_{2/3}Nb_{1/3}$) one (14).

Lead titanate ($PbTiO_3$, PT) is a classical ferroelectric. The La modification of PT (PLT) induces relaxor behavior for a La content of about 25 at.% compared to Pb. The authors supposed that the large amount of La that is required to induce the relaxor behavior is probably a reflection of the large initial lattice distortion ($c/a \sim 1.063$) (15). In highly doped samples, X-ray measurements indicate a cubic structure, although measurements of Raman scattering at temperatures above and below the tetragonal-to-cubic transformation showed a residual short-range structural disorder in the cubic phase (16). This suggests a relationship between local disorder and relaxor behavior in this system.

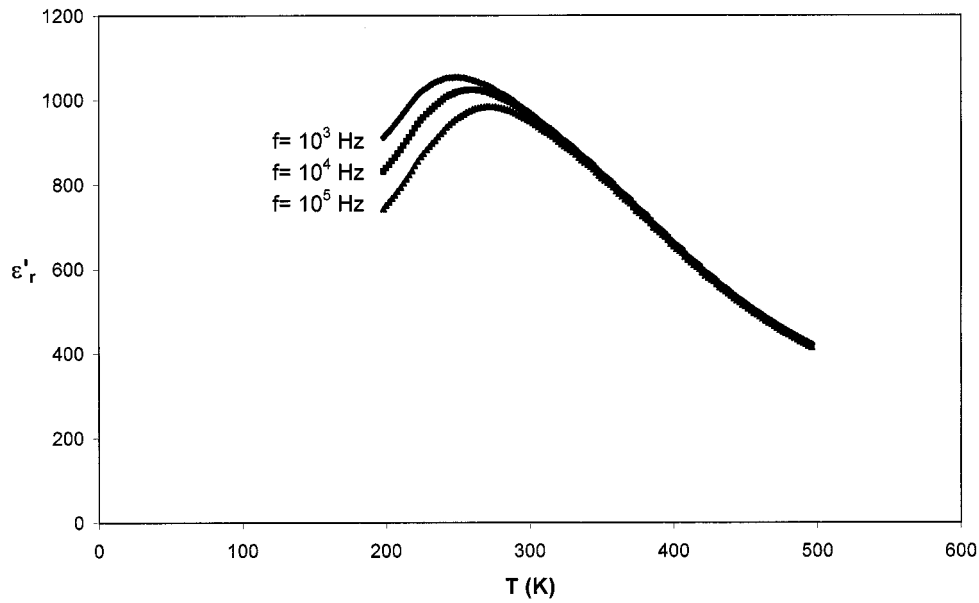

FIG. 6. Temperature dependence of ε_r' at various frequencies for $Pb_4BaTa_{10}O_{30}$ composition.

TABLE 5
Interatomic Distances in $Pb_{4.25}La_{0.5}Ta_{10}O_{30}$ (Bold) and in $Pb_{4.5}KTa_{10}O_{30}$

Bond	Length (Å)	Bond	Length (Å)
Ta(1)–O(1) (× 4)	**1.91(1)**	Pb(2)–O(3) (× 2)	**2.79(1)**
	1.95(2)		2.83(1)
Ta(1)–O(4) (× 2)	**1.94(1)**	Pb(2)–O(4)	**3.013(3)**
	1.95(1)		3.010(4)
Ta(2)–O(1)	**1.97(2)**	Pb(2)–O(5)	**3.76(2)**
	1.94(2)		3.81(2)
Ta(2)–O(2)	**2.06(2)**	Pb(2)–O(5)	**3.38(2)**
	2.08(2)		3.45(2)
Ta(2)–O(2)	**1.86(2)**	Pb(2)–O(5)	**2.99(2)**
	1.89(2)		3.01(2)
Ta(2)–O(3)	**2.01(2)**	Pb(2)–O(5)	**3.14(2)**
	2.00(3)		3.10(2)
Ta(2)–O(5) (× 2)	**1.937(1)**	**La(1)–O(1) (×4)**	**3.30(2)**
	1.951(1)	K(1)–O(1) (× 4)	3.37(4)
Pb(1)–O(2) (× 8)	**2.70(2)**	**La(1)–O(2) (×4)**	**3.30(2)**
	2.74(1)	K(1)–O(2) (× 4)	3.30(4)
Pb(1)–O(5) (× 4)	**2.77(2)**	**La(1)–O(3) (×2)**	**2.32(2)**
	2.80(2)	K(1)–O(3) (× 2)	2.30(4)
Pb(2)–O(1) (× 2)	**3.01(2)**	**La(1)–O(4)**	**3.71(2)**
	3.05(2)	K(1)–O(4)	3.79(4)
Pb(2)–O(1) (× 2)	**2.71(1)**	**La(1)–O(5) (×2)**	**3.74(3)**
	2.70(1)	K(1)–O(5) (× 2)	3.80(4)
Pb(2)–O(2) (× 2)	**3.12(1)**	**La(1)–O(5) (×2)**	**2.64(3)**
	3.08(1)	K(1)–O(5) (× 2)	2.60(4)
Pb(2)–O(2) (× 2)	**3.63(2)**		
	3.68(2)		

This introduction of lanthanum in the PT matrix perturbs the long-range Coulomb interactions, inhibits the formation of ferroelectric domains, and leads to polar microdomains (17).

Compositions of PZT with the general formula $Pb(Zr_{1-x}Ti_x)O_3$ are classical ferroelectrics. Relaxor behavior was shown to be induced for certain Zr/Ti ratios by a Pb–La substitution (PLZT) and the La amount required was observed to increase with increasing Ti content (15). This phenomenon was correlated to the evolution of the c/a ratio, i.e., the tetragonal distortion. In this study, La atoms are considered as quenched impurities. These defects, which are randomly quenched, locally lower the symmetry and interrupt the long-range dipolar interactions within the domains. Consequently, domain evolution cannot occur upon cooling; rather polar nanodomains are metastably trapped, resulting in the relaxor behavior (18, 19).

Furthermore, concerning these three examples (PLMN, PLT, and PLZT), the lanthanum substitution in the A site of the perovskite structure also leads to a decrease of T_C or T_m.

The results obtained in our study are in full agreement with those developed above: the lanthanum insertion in the $Pb_5Ta_{10}O_{30}$ matrix ($Pb_{5(1-x)}La_{10x/3}Ta_{10}O_{30}$) induces relaxor behavior from $x = 0.10$ and the amplitude of this phenomenon (ΔT_m) increase with increasing La content. Furthermore, it also leads to a decrease of T_C or T_m. The existence of the relaxor behavior in the studied lanthanum-containing compositions is not related to a problem with unbalanced electrical charges as in PLMN. In fact, lanthanum atoms can be considered defects, which from a certain content, perturb the long-range polarization and induce thus relaxor behavior. This study permits an important point to be emphasized: the influence of the Pb–La substitution on the ferroelectric properties is identical, whatever the structure (perovskite or TTB).

Potassium-containing compositions. Few studies concern the influence of Pb–K substitution on the ferroelectric properties. Investigations of PZT compositions modified by potassium (PKZT) have not shown relaxor behavior, even if the transition becomes more and more diffuse. As charge

TABLE 6
Powder Crystallographic Data, Experimental Conditions, and Rietveld Data for $Pb_{4.5}Ba_{0.5}Ta_{10}O_{30}$ and $Pb_{4.5}Ca_{0.5}Ta_{10}O_{30}$

	$Pb_{4.5}Ca_{0.5}Ba_{0.5}Ta_{10}O_{30}$	$Pb_{4.5}Ca_{0.5}Ta_{10}O_{30}$
Crystallographic data		
Symmetry	Tetragonal	Orthorhombic
Existence conditions	$(0kl)$ $k = 2n$	$(0kl)k=2n,(h01)h=2n$
Space group	$P4bm$ (No. 100)	$Pbam$ (No. 55)
Unit-cell parameters (Å)	$a = b = 12.5106(1)$	$a = 12.5084(4)$
		$b = 12.4079(4)$
	$c = 3.8849(1)$	$c = 3.8617(1)$
Volume (Å^3)	$V = 608(1)$	$V = 559.3(1)$
Experimental conditions for data collection		
Radiation	CuKα ($l = 1.5418$ Å)	
Measuring range	$10^\circ < 2\theta < 120^\circ$	
Step	0.02°	
Integration time	30 s	
Rietveld data		
Program for Rietveld analysis	Fullprof	
Number of independent reflections	286	529
Number of independent parameters	33	42
Function for background level	Polynomial (5 order)	Polynomial (5 order)
Function for peak shape	Pseudo-Voigt	Pseudo-Voigt
($H^2 = U\tan^2\theta + V\tan\theta + W$)	$U = 0.020(2)$	$U = 0.061(7)$
	$V = 0.002(2)$	$V = -0.013(5)$
	$W = 0.003(1)$	$W = 0.007(1)$

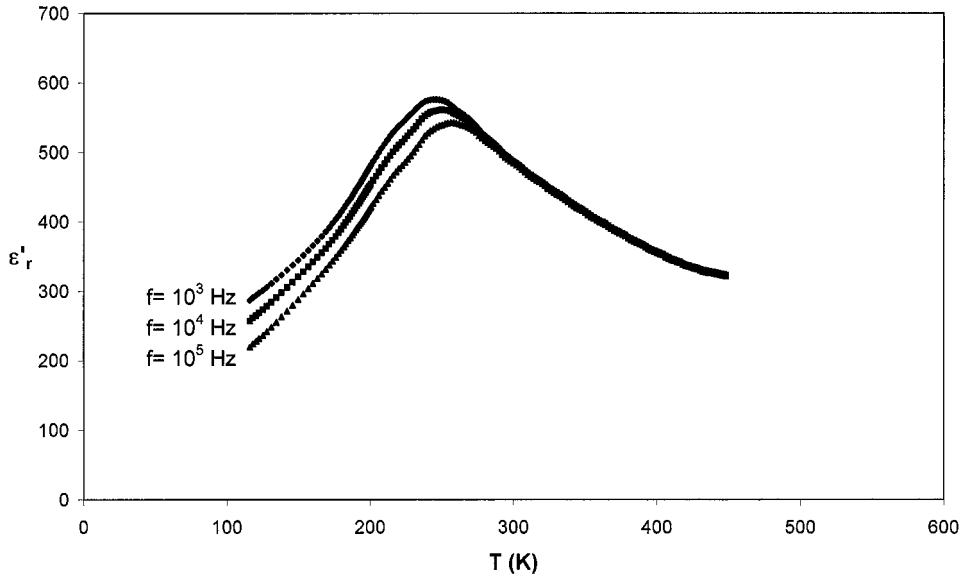

FIG. 7. Temperature dependence of ε_r' at various frequencies for $Pb_{4.5}Ca_{0.5}Ta_{10}O_{30}$ composition.

compensation occurs dominantly by the creation of oxygen vacancies, which are mobile, potassium atoms are considered mobile impurities, which diffuse to domain boundaries and order in chain fragments. A coupling between chain fragments and boundaries results thus in a polarization pinning as well as a wavy domain morphology (20).

Two compositions with a tetragonal tungsten bronze structure containing lead and potassium were also investigated in crystallographic and dielectric studies: $Pb_4K_2Ta_{10}O_{30}$ and $Pb_4K_2Nb_{10}O_{30}$ (11, 21).

The first one is a relaxor ferroelectric that presents a T_m value equal to 206 K at 10^3 Hz and a value of ΔT_m close to 20 K (22). Crystallographic data determined at room

TABLE 7
Atomic Coordinates, Isotropic Thermal Parameters B (Å²), and Occupancies (*p*) in $Pb_{4.5}Ba_{0.5}Ta_{10}O_{30}$

Atoms	Theoretical valence	Wyckoff site	*x*	*y*	*z*	*B*	*p*
Ta(1)	+ 5	2*b*	0	0.5	0.482(7)	0.14(7)	1
Ta(2)	+ 5	8*d*	0.0730(1)	0.2097(1)	0.472(5)	0.06(3)	1
Pb(1)	+ 2	2*a*	0	0	0**	1.0(2)	0.532(1)
Pb(2)	+ 2	8*d*	0.1882(3)	0.6504(3)	–0.001(8)	2.6(1)	0.422(1)
Ba(1)	+ 2	4*c*	0.211(2)	0.711(2)	–0.001(8)	2.6(1)	0.124(3)
O(1)	− 2	8*d*	0.358(2)	0.002(1)	0.5**	3.2(3)*	1
O(2)	− 2	8*d*	0.148(2)	0.060(2)	0.5**	3.2(3)*	1
O(3)	− 2	4*c*	0.280(1)	0.780(1)	0.5**	3.2(3)*	1
O(4)	− 2	2*b*	0	0.5	0**	3.2(3)*	1
O(5)	− 2	8*d*	0.083(2)	0.208(1)	0**	3.2(3)*	1

Note. * denotes average value refined for oxygen atoms. ** denotes fixed values.

TABLE 8
Interatomic Distances in $Pb_{4.5}Ba_{0.5}Ta_{10}O_{30}$

Bond	Length (Å)	Bond	Length (Å)
Ta(1)–O(1) (× 4)	1.79(2)	Pb(2)–O(3) (× 2)	2.78(2)
Ta(1)–O(4)	1.87(3)	Pb(2)–O(4)	3.014(3)
Ta(1)–O(4)	2.01(3)	Pb(2)–O(5)	3.16(2)
Ta(2)–O(1)	2.08(2)	Pb(2)–O(5)	3.79(2)
Ta(2)–O(2)	2.10(2)	Pb(2)–O(5)	3.38(2)
Ta(2)–O(2)	1.83(2)	Pb(2)–O(5)	2.98(2)
Ta(2)–O(3)	2.04(2)	Ba(1)–O(1) (× 4)	3.37(3)
Ta(2)–O(5)	1.84(2)	Ba(1)–O(2) (× 4)	3.23(3)
Ta(2)–O(5)	2.05(2)	Ba(1)–O(3)	2.29(3)
Pb(1)–O(2) (× 8)	2.79(2)	Ba(1)–O(3)	2.30(3)
Pb(1)–O(5) (× 4)	2.79(2)	Ba(1)–O(4)	3.73(2)
Pb(2)–O(1) (× 2)	3.03(3)	Ba(1)–O(5) (× 2)	3.78(3)
Pb(2)–O(1) (× 2)	2.75(2)	Ba(1)–O(5) (× 2)	2.61(3)
Pb(2)–O(2) (× 2)	3.04(2)		
Pb(2)–O(2) (× 2)	3.56(2)		

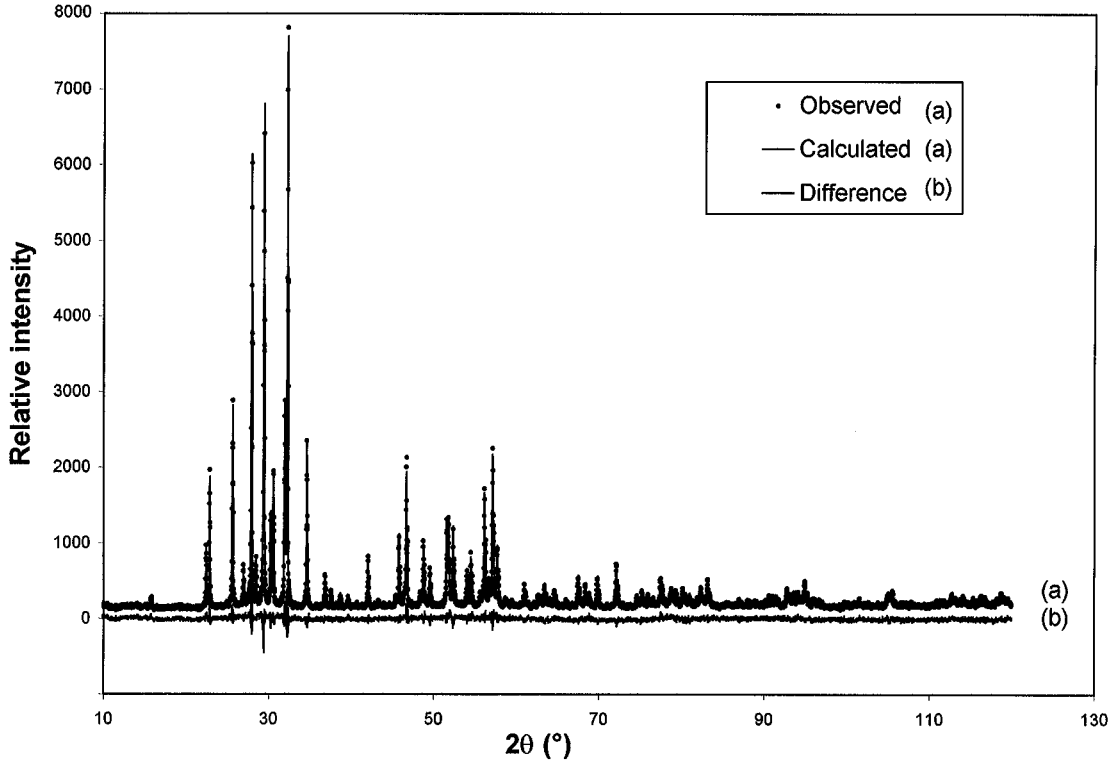

FIG. 8. X-ray diffraction patterns for $Pb_{4.5}Ba_{0.5}Ta_{10}O_{30}$ composition.

temperature are in very good agreement with those obtained for the $Pb_{4.5}KTa_{10}O_{30}$ composition. As the temperature decreases from the paraelectric phase to the ferroelectric one, the X-ray diffraction patterns do not exhibit any significant change; the composition remains in the tetragonal symmetry, whatever the temperature. In contrast, the second composition, $Pb_4K_2Nb_{10}O_{30}$, is a classical ferroelectric. The difference between the tantalate

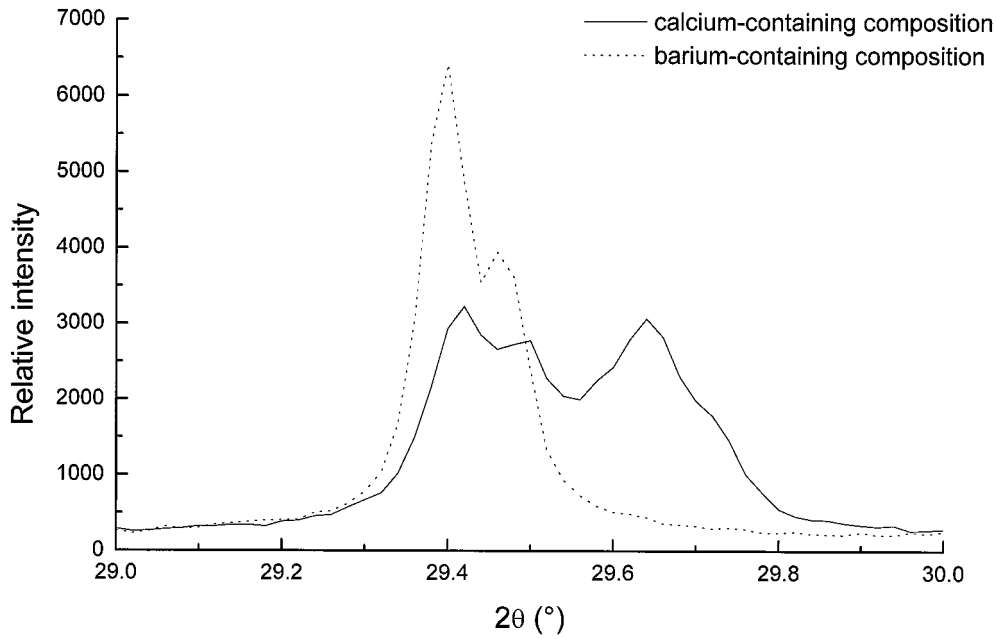

FIG. 9. Evidence of the orthorhombic symmetry for the $Pb_{4.5}Ca_{0.5}Ta_{10}O_{30}$ composition (zoom in the [29°–30°] 2θ region).

TABLE 9
Atomic Coordinates, Isotropic Thermal Parameters B (Å^2), and Occupancies (p), in $Pb_{4.5}Ca_{0.5}Ta_{10}O_{30}$

Atoms	Theoretical valence	Wyckoff site	x	y	z	B	p
Ta(1)	+ 5	2*d*	0	0.5	0.5	0.29(9)	1
Ta(2)	+ 5	4*h*	0.0724(2)	0.2100(2)	0.5	0.18(7)	1
Ta(3)	+ 5	4*h*	0.2078(2)	0.9230(2)	0.5	0.18(7)	1
Pb(1)	+ 2	2*a*	0	0	0	0.7(2)	0.404(1)
Pb(2)	+ 2	4*g*	0.1936(3)	0.6539(3)	0	3.1(1)	0.880(1)
Ca(1)	+ 2	4*g*	0.238(6)	0.686(6)	0	3.1(1)	0.120(9)
O(1)	− 2	4*h*	0.347(3)	− 0.013(3)	0.5	3.2(3)*	1
O(2)	− 2	4*h*	0.009(3)	0.648(3)	0.5	3.2(3)*	1
O(3)	− 2	4*h*	0.124(3)	0.048(3)	0.5	3.2(3)*	1
O(4)	− 2	4*h*	0.066(3)	0.859(3)	0.5	3.2(3)*	1
O(5)	− 2	4*h*	0.293(3)	0.784(2)	0.5	3.2(3)*	1
O(6)	− 2	2*c*	0	0.5	0	3.2(3)*	1
O(7)	− 2	4*g*	0.085(3)	0.197(3)	0	3.2(3)*	1
O(8)	− 2	4*g*	0.199(3)	0.940(3)	0	3.2(3)*	1

Note. * denotes the average value refined for oxygen atoms.

(relaxor ferroelectric) and the niobate (classical ferroelectric) was explained by the authors in terms of the origin of polarization. In fact, ferroelectric polarization in the niobate is supposed to be due to both the Pb off-site position and Nb displacements, whereas in the tantalate, the polarization seems to be only due to Pb atoms. In the latter, the Pb–K substitution should weaken the correlations between the Pb atoms and consequently suppress the ferroelectric transition.

The $Pb_4K_2Ta_{10}O_{30}$ composition that corresponds to $x = 0.20$ in our study allowed us to note that the insertion of potassium in the $Pb_5Ta_{10}O_{30}$ matrix induces relaxor behavior, which seems weakly dependent on the substitution rate (evolution of ΔT_m as a function of composition).

3.2. Homovalent Substitutions: $Pb^{2+} \rightarrow Ba^{2+}$ and $Pb^{2+} \rightarrow Ca^{2+}$

The two cations Ba^{2+} and Ca^{2+} were chosen because of their difference in ionic radius (C.N. 12) ($r[Ba^{2+}] = 1.61$ Å, $r[Ca^{2+}] = 1.34$ Å, and $r[Pb^{2+}] = 1.49$ Å) (8).

3.2.1. Ferroelectric Properties

The temperature dependence of ε'_r at various frequencies has shown that $Pb_{4.5}Ba_{0.5}Ta_{10}O_{30}$ is a classical ferroelectric ($T_C = 380$ K), whereas $Pb_4BaTa_{10}O_{30}$ and $Pb_{4.5}Ca_{0.5}$ $Ta_{10}O_{30}$ are relaxor ferroelectrics associated with a value of T_m (at 10^3 Hz) equal to 250 and 240 K and to a value of ΔT_m equal to 20 and 12 K, respectively (Figs. 6 and 7).

3.2.2. Structure Determination and Refinements

$Pb_{4.5}Ba_{0.5}Ta_{10}O_{30}$. Even if this composition does not show relaxor behavior, it was chosen for a comparison at the end of the study of the influence of each type of substitution for a constant lead content. First, all diffraction lines were indexed on the basis of tetragonal symmetry. The reflection condition [$(0kl)$ $k = 2n$] is the same as those determined previously. Because the Curie temperature of this sample is 380 K, the powder X-ray diffraction data were recorded in the ferroelectric phase. The structure was thus refined in the noncentrosymmetric polar space group *P*4*bm*. The powder data and experimental conditions are given in Table 6.

As for the two previous compositions ($Pb_{4.25}La_{0.5}$ $Ta_{10}O_{30}$ and $Pb_{4.5}KTa_{10}O_{30}$), the *A*1 sites are only occupied by lead atoms in a normal position (2*a*) whereas *A*2 sites are occupied by either barium [normal position (4*c*)] or lead [shifted position (8*d*)]. The accuracy on the z position for this polar space group is very poor, even for heavy atoms such as tantalum or lead, so those of oxygen atoms were not refined. The corresponding reliability factors were $R_{Bragg} = 7.9\%$, $cR_p = 17.7\%$, $R_F = 8.4\%$, and $\chi^2 = 1.96$.

TABLE 10
Interatomic Distances in $Pb_{4.5}Ca_{0.5}Ta_{10}O_{30}$

Bond	Length (Å)	Bond	Length (Å)
Ta(1)–O(1) (× 2)	1.91(3)	Pb(2)–O(1) (× 2)	2.88(2)
Ta(1)–O(2) (× 2)	1.84(4)	Pb(2)–O(2) (× 2)	3.01(3)
Ta(1)–O(6) (× 2)	2.93(1)	Pb(2)–O(3) (× 2)	3.27(3)
Ta(2)–O(2)	2.03(4)	Pb(2)–O(4) (× 2)	3.57(3)
Ta(2)–O(3)	2.11(4)	Pb(2)–O(5) (× 2)	2.81(2)
Ta(2)–O(7) (× 2)	1.94(1)	Pb(2)–O(6)	3.08(1)
Ta(3)–O(1)	1.92(3)	Pb(2)–O(7)	2.82(3)
Ta(3)–O(3)	1.88(4)	Pb(2)–O(7)	3.95(3)
Ta(3)–O(4)	1.94(4)	Pb(2)–O(8)	3.55(4)
Ta(3)–O(5)	2.02(3)	Pb(2)–O(8)	2.98(4)
Ta(3)–O(8) (× 2)	1.95(1)	Ca(1)–O(1) (× 2)	3.31(7)
Pb(1)–O(3) (× 4)	2.55(2)	Ca(1)–O(2) (× 2)	3.48(7)
Pb(1)–O(4) (× 4)	2.73(3)	Ca(1)–O(3) (× 2)	3.11(7)
Pb(1)–O(7) (× 2)	2.67(3)	Ca(1)–O(4) (× 2)	3.60(7)
Pb(1)–O(8) (× 2)	2.60(4)	Ca(1)–O(5) (× 2)	2.38(5)
		Ca(1)–O(6)	3.77(7)
		Ca(1)–O(7)	2.21(8)
		Ca(1)–O(7)	4.29(8)
		Ca(1)–O(8)	3.18(8)
		Ca(1)–O(8)	3.16(8)

The final positional coordinates and the final atomic displacements corresponding to the best models are listed in Table 7 and the interatomic distances are given in Table 8. The observed and calculated X-ray diffraction patterns as well as their differences are presented in Fig. 8.

$Pb_{4.5}Ca_{0.5}Ta_{10}O_{30}$. The X-ray powder diffraction pattern of $Pb_{4.5}Ca_{0.5}Ta_{10}O_{30}$ can be completely indexed with an orthorhombic unit cell (Fig. 9 illustrates the orthorhombic distortion). The existence conditions [$(0kl)$ $k = 2n$ and $(h0l)$ $l = 2n$] and the value of T_m ($T_m = 245 < 298$ K) have permitted selection of the centrosymmetric space group *Pbam*. Powder data and experimental conditions are listed in Table 6. Results of refinement indicate that each $A1$ site is only occupied by lead atoms, whereas $A2$ sites are occupied by either lead or calcium atoms (Table 9). We can note that atomic coordinates (x, y) of lead and calcium atoms are significantly different in this $A2$ site. This phenomenon should be responsible for the symmetry change observed from $Pb_5Ta_{10}O_{30}$ to $Pb_{4.5}Ca_{0.5}Ta_{10}O_{30}$. The reliability factors corresponding to the best model are $R_{Bragg} = 7.3\%$, $cR_p = 16.7\%$, $R_F = 5.7\%$, and $\chi^2 = 2.42$.

Even if the refinement converges and the corresponding reliability factors are satisfactory, the position of calcium atoms in $A2$ sites is not accurate. This atom is certainly displaced from the average obtained position, leading to widely distributed Ca–O bonds (Table 10).

3.2.3. Discussion

Barium-containing compositions. Most of the studies of lead-containing compositions where a part of lead atoms are replaced by barium ones concerns the $Pb_{1-x}Ba_xNb_2O_6$ ($0 < x < 0.80$) system with a TTB-type structure (23). This solid solution possesses a morphotropic phase boundary (MPB) between orthorhombic and tetragonal ferroelectric phases. The largest frequency dispersion (relaxor behavior) occurs at the MPB of $1 - x = 0.63$ associated with the lowest Curie temperature (24). The origin of the relaxor behavior was explained here by Guo *et al.* using a new mechanism: the thermally agitated local polarization fluctuation model (25, 26). It is strongly based on the superparaelectric theory and on the existence of two different polarization orientations due to the morphotropic phase boundary. The local chemical fluctuations of Ba^{2+} and Pb^{2+} in the $A2$ site are sensitive to the perturbation of the polarization. This perturbation is not only a change in magnitude but also an orientation deviation. The latter results from the two orthogonal polarization orientations that can occur at either side of the MPB. Relaxor ferroelectrics are considered as originating from a polar matrix with local perturbations but not from local polar microregions in a paraelectric matrix. The effect of A-site vacancy order–disorder states on diffuse phase transition was studied by Xiao *et al.* (27). It was shown that ordered PBN ceramics gave weak dispersion compared to disordered ones. The latter contain more structural distortions and defects that tend to lower local symmetry.

The influence of barium substitution in lead-containing ferroelectric or antiferroelectric perovskite compounds was also evidenced. Concerning the $Pb(Fe_{1/2}Nb_{1/2})O_3$ compound and the $Pb_{1-x}Ba_xZrO_3$ ($x \leq 0.25$) solid solution, relaxor behavior was induced by barium insertion (28, 29).

Results obtained in the present study are in agreement with those described in the literature: Pb–Ba substitution strongly modifies dielectric properties. A diminution of T_C or T_m is provoked and relaxor behavior is induced. It can be noted that Pb^{2+} and Ba^{2+} cations possess a different electronic configuration: Pb^{2+} (lone pair $6s^2$) and Ba^{2+} (filled shell); this could induce heterogeneities of polarization.

Calcium-containing composition. The $Pb_{1-x}Ca_xTiO_3$ system was the subject of thorough investigations from a structural and a dielectric point of view. A partial ordering of lead and calcium atoms was evidenced for compositions corresponding to $0.30 \leq x \leq 0.60$ (30). In this study, the

dielectric measurements do not reveal the existence of any relaxor behavior, even if the addition of calcium titanate broadens the width of the phase transition. In a different study concerning the $Pb_{4.5}Ca_{0.5}TiO_3$ composition, Ranjan *et al.* evidenced superlattice reflections due to an orthorhombic distortion that results from tilted TiO_6 octahedra and an off-center location of Pb^{2+} and Ca^{2+} (31). The temperature dependence of the real and imaginary parts of the dielectric constant at various frequencies show that this composition is a relaxor ferroelectric. It was proposed that the structural frustation introduced by the tilted octahedra may be responsible for the relaxor behavior.

their normal position (except for the calcium-containing composition).

Furthermore, it was shown that whatever the substitution considered, relaxor behavior is induced by replacing a small amount of Pb^{2+} by La^{3+}, K^+, and Ca^{2+} in the $Pb_5Ta_{10}O_{30}$ matrix. A larger amount is necessary in the case of the $Pb^{2+} \rightarrow Ba^{2+}$ substitution.

The following diagram collects data obtained for different compositions but with a constant lead concentration. The theoretical valence (V), the ionic radius (r/Å) with coordination number 12, and the ferroelectric behavior are reported.

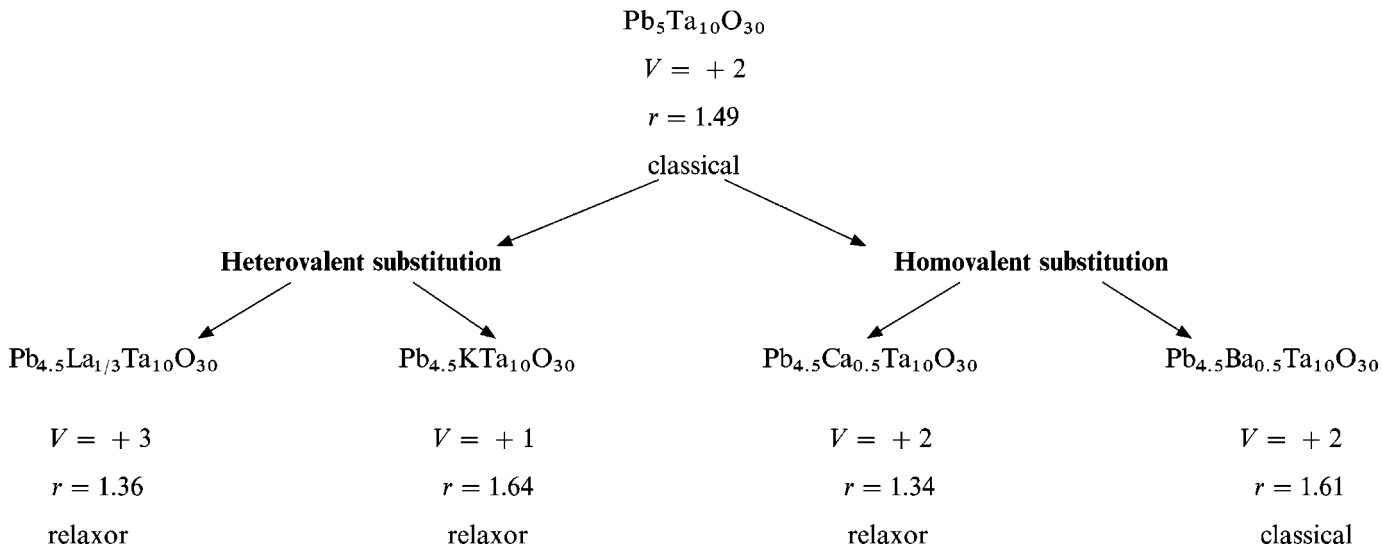

When Ca^{2+} is substituted for Ba^{2+} in $BaTi_{0.75}Zr_{0.25}O_3$ composition, relaxor behavior was found and was attributed to supplementary local polarization resulting from the Ca^{2+} displacement in its crystallographic site (32).

The composition $Pb_{4.5}Ca_{0.5}Ta_{10}O_{30}$ studied in this work exhibits similar behavior. In fact, for a low rate of substitution, on the one hand, the T_m value is dramatically decreased and, on the other hand, relaxor behavior appears. The displacement of Ca^{2+} in its crystallographic site seems to be a common feature as well as an orthorhombic distortion. The relaxor behavior is thus probably related principally to a steric effect.

4. GENERAL DISCUSSION AND CONCLUSION

Structure determinations and refinements have permitted determination of the crystallographic site occupied by La^{3+}, K^+, Ba^{2+}, and Ca^{2+}. For all substitutions under consideration, these cations occupy the $A2$ site with coordination number 15 and the corresponding bond lengths involving oxygen atoms are widely distributed. The position of the cation in the $A2$ site is different from that of lead atoms. Furthermore, Pb^{2+} cations are displaced from

The apparent valence of Pb^{2+} cations in the $A2$ site (15-coordination) for $Pb_{4.5}La_{1/3}Ta_{10}O_{30}$, $Pb_{4.5}KTa_{10}O_{30}$, and $Pb_{4.5}Ba_{0.5}Ta_{10}O_{30}$ compositions was calculated using the program "Valence" (33). It is clear from values obtained (between 1.31 and 1.36) that the Pb^{2+} cations in the considered site are severely underbonded. This result was also reported in the structure analysis performed on a $Pb_{0.596}Ba_{0.404}Nb_{2.037}O_6$ single crystal (34). This phenomenon is thus observed for relaxor as much as it is for classical ferroelectric compositions. It clearly shows that the relaxor behavior is due to not only lead atoms and but also cations occupying the same crystallographic site ($A2$) that have a strong influence. If the cation exhibits a difference in charge and/or ionic radius (La^{3+} and K^+), relaxor behavior is induced for a low rate of substitution. The local disorder is sufficiently important to inhibit the existence of a long-range polar order. Concerning barium-containing compositions, a greater rate of substitution is necessary to provoke the relaxor behavior ($Pb_4BaTa_{10}O_{30}$). This demonstrates that the chemical nature of each cation must be taken into account. The study of this supplementary effect is in progress by way of experimental and calculated electron density for several compositions.

REFERENCES

1. T. Egami, S. Teslic, W. Dmowski, D. Viehland, and S. Vakhrushev, *Ferroelectrics* **199,** 103 (1997)
2. T. Egami, D. Dmowski, S. Teslic, P. K. Davies, I.-W. Chen, and H. Chen, *Ferroelectrics* **206,** 231 (1998).
3. B. Dkhil, *Thesis*, University of Paris XI, 1999.
4. V. Hornebecq, C. Elissalde, F. Weill, A. Villesuzanne, M. Menetrier, and J. Ravez, *J. Appl. Crystallogr.* **33,** 1037 (2000).
5. E. C. Subbarao, G. Shirane, and F. Jona, *Acta Crystallogr.* **13,** 226 (1958).
6. V. Hornebecq, J. M. Reau, and J. Ravez, *Solid State Ionics* **127,** 231 (2000).
7. H. M. Rietveld, *J. Appl. Crystallogr.* **2,** 65 (1969).
8. R. D. Shannon, *Acta Crystallogr. A* **32,** 751 (1976).
9. J. Rodriguez-Carvajal, *in* "Collected Abstracts of Powder Diffraction Meeting." Toulouse France, p. 127. 1990.
10. G. Caglioti, A. Paoletti, and F. P. Ricci, *Nucl. Instrum. Methods* **3,** 223 (1958).
11. P. Sciau, G. Calvarin, T. Roisnel, and J. Ravez, *Mater. Res. Bull.* **28,** 1233 (1993).
12. N. de Mathan, E. Husson, P. Gaucher, and A. Morell, *Mater. Res. Bull.* **25,** 427 (1990).
13. N. de Mathan, E. Husson, and A. Morell, *Mater. Res. Bull.* **27,** 867 (1992).
14. D. M. Fanning, I. K. Robinson, S. T. Jung, E. V. Colla, D. D. Viehland, and D. A. Payne, *J. Appl. Phys.* **87,** 840 (2000).
15. X. Dai, Z. Xu, and D. Viehland, *J. Appl. Phys.* **79,** 1021 (1996).
16. E. C. S. Tavares, P. S. Pizani, and J. A. Eiras, *Appl. Phys. Lett.* **72,** 897 (1998).
17. O. Bidault, *Thesis*, University of Bourgogne, 1995.
18. Q. Tan, Z. Xu, J. F. Li, and D. Viehland, *Appl. Phys. Lett.* **71,** 1062 (1997).
19. D. Viehland, X. H. Dai, J. F. Li, and Z. Xu, *J. Appl. Phys.* **84,** 458 (1998).
20. Q. Tan, J. F. Li, and D. Viehland, *Philos. Mag. B* **76,** 58 (1997).
21. P. Sciau, G. Calvarin, and J. Ravez, *Acta. Crystallogr. B* **55,** 459 (1999).
22. Z. G. Lu, J.-P. Bonnet, J. Ravez, and P. Hagenmuller, *Eur. J. Solid State Inorg. Chem.* **30,** 817 (1993).
23. T. R. Shrout, H. Chen, and L. E. Cross, *Ferroelectrics* **56,** 45 (1983).
24. J. R. Oliver, R. R. Neurgaonkar, and L. E. Cross, *J. Am. Ceram. Soc.* **72,** 202 (1989).
25. R. Guo, A. S. Bhalla, C. A. Randall, Z. P. Chang, and L. E. Cross, *J. Appl. Phys.* **67,** 1453 (1990).
26. R. Guo, A. S. Bhalla, C. A. Randall, and L. E. Cross, *J. Appl. Phys.* **67,** 6405 (1990).
27. X. Xiao, Y. Xu, Z. Zeng, Z. Gui, L. Li, and X. Zhang, *J. Mater. Res.* **11,** 2302 (1996).
28. M. V. R. Rao and A. M. Umarji, *J. Mater. Sci. Lett.* **18,** 59 (1999).
29. Z. Ujma, J. Handerek, M. Pawelczyk, and D. Dmytrow, *Ferroelectrics* **129,** 217 (1992).
30. R. Ganesh and E. Goo, *J. Am. Ceram. Soc.* **80,** 653 (1997).
31. R. Ranjan, N. Singh, D. Pandey, V. Siruguri, P. S. R. Krishna, S. K. Paranjpe, and A. Banerjee, *Appl. Phys. Lett.* **70,** 3221 (1997).
32. P. Sciau, G. Calvarin, and J. Ravez, *Solid State Commun.* **113,** 77 (2000).
33. L. D. Brown and D. Altermatt, *Acta Crystallogr.* **41,** 244 (1985).
34. R. Guo, H. T. Evans, and A. S. Bhalla, *Ferroelectrics* **206–207,** 123 (1998).